Influence of various growth parameters on the interface abruptness of AlAs/GaAs short period superlattices

A. R. Smith, Kuo-Jen Chao, and C. K. Shih[a)]
Department of Physics, The University of Texas at Austin, Austin, Texas 78712

Y. C. Shih, K. A. Anselm, and B. G. Streetman
Department of Electrical and Computer Engineering, The University of Texas at Austin, Austin, Texas 78712

(Received 25 January 1995; accepted 18 April 1995)

Cross-sectional scanning tunneling microscopy has been used to investigate the effects of several key growth parameters on the resulting interfacial quality of AlAs/GaAs short period superlattices. For growth on top of AlGaAs layers, only superlattices grown with periodicity no smaller than 4 unit cells of GaAs and 2 unit cells of AlAs and grown with a minimum of 30 s of growth interrupt time are resolved. On the other hand, when grown on top of GaAs layers, superlattices as fine as 2 unit cells of GaAs and 1 unit cell of AlAs grown with only 5 s of growth interrupt time are resolved. This result suggests that the material on which the superlattice is grown is at least as important as the growth interrupt time. In particular, GaAs seems to provide a smoother starting surface than AlGaAs and hence aids in the formation of abrupt interfaces. We also compare our scanning tunneling microscopy data with some predictions based on simple atomic models of the interfacial regions.

I. INTRODUCTION

Short period superlattices are a novel class of materials which have great potential for use in device applications.[1,2] Applicability of these structures for use in electronics and optoelectronics depends on the ability to grow them with atomically abrupt interfaces. In order to assess the quality of grown superlattices, a number of techniques have been applied. However, the tool which is most suitable for directly measuring the interface abruptness at the atomic scale is the method of cross-sectional scanning tunneling microscopy (XSTM).

In the past, this method has been applied to the study of compound semiconductor heterostructures and their interfaces, particularly in the case of the AlGaAs/GaAs system.[3–6] But this method is by no means limited to a given material system, as recent work has shown.[5] By applying a combination of XSTM and scanning tunneling spectroscopy (STS), a new and powerful technique, XSTM/S, has emerged for investigating not only the structural but also the electronic properties of heterostructures and their interfaces.[3,6–10]

Recent work using this technique on superlattices in particular has focused on interface roughness and interface roughness asymmetry effects.[11,12] The amount of roughness can be related to steps on the growth surface and also intermixing at the interfaces. Roughness asymmetry can arise from variations in the nature of the growth surface for different materials. This situation can become even more complex for mixed-anion superlattices in which two types of interfaces can result, for example in the case of InAs/GaSb. These interfaces are referred to as either ''InSb-like'' or ''GaAs-like'' depending on the particular bonding configurations at the interfaces. But in the case of common-anion superlattices, such as in the present case of AlAs/GaAs, the situation is greatly simplified. This makes the AlAs/GaAs system ideal for investigating interface abruptness.

It is well known that interface roughness can have a major impact on device performance. This is especially true in the case of short period superlattices in which the roughness is on the same length scale as a single superlattice period. Clearly, it is vital to understand the influence of various growth parameters on the resulting interfacial roughness of a grown device. In a recent investigation of short period superlattices, we found that it was possible to delineate GaAs/AlAs superlattices with periodicity as small as 4 unit cells of GaAs and 2 unit cells of AlAs grown using a 30 s growth interrupt on top of a layer consisting of $Al_{0.3}Ga_{0.7}As$.[13] At the interfaces, there was an apparent intermixing over about a single unit cell. However, superlattices of the same periodicity, but grown with a smaller amount of growth interrupt time (5 s), could not be differentiated from ternary AlGaAs regions; neither could superlattices having even smaller periodicity. These results strongly suggested the importance of the growth interrupt time.

In the current work, we have extended this growth parameter study to include the material upon which the superlattices are grown by growing them on top of GaAs layers. We find that this has a beneficial effect on the resulting interface quality, allowing us to observe all the superlattices which were unobservable previously when grown on top of AlGaAs.

II. EXPERIMENT

Our experiments are performed inside an ultrahigh vacuum (UHV) chamber with a base pressure of less than 4×10^{-11} Torr. Tips are electrochemically etched and treated in the vacuum using one of two methods. In the first method, field emission of the tip is performed on separate clean substrates. In the second method, the tip is cleaned using an

a)Author to whom correspondence should be addressed.

electron-beam heating technique. Both methods yield tips giving atomic resolution in the heterojunction regions. Samples are grown *p*-type at 10^{19} cm^{-3}[Be] using molecular beam epitaxy on *p*-type [001]-oriented wafers. Typical wafer thickness is 0.35 mm. A cleavage mark is scribed on part of the epilayer side, and the sample is pushed along the [001] direction in order to cleave. Cleavage is performed in UHV.

In our study of short period superlattices, we have focused on three key growth parameters which influence interface abruptness. First, we varied the periodicity and studied superlattices composed of the following: (a) 4 unit cells of GaAs (22.6 Å) followed by 2 unit cells of AlAs (11.3 Å) denoted as (4/2) and (b) 2 unit cells of GaAs (11.3 Å) followed by 1 unit cell of AlAs (5.66 Å) denoted as (2/1). Second, we varied the amount of growth interrupt time imposed at each interface of the superlattice. Typical growth interrupt times were 5 s and 30 s. Third, we varied the material on which the superlattice layers were grown by growing on top of both AlGaAs and GaAs.

In our first set of samples (sample type 1) grown at 580 °C, all but one of the superlattices were grown on top of AlGaAs layers. The device structure consisted of 10 repetitions of the (4/2) structure and 10 repetitions of the (2/1) structure Each of these superlattices was grown twice, once using a 5 s growth interrupt and once using a 30 s growth interrupt. Thus, altogether four unique superlattices were grown, each one also followed by 500 Å of $Al_{0.3}Ga_{0.7}As$. All of this was grown on top of a 6-μ thick region of alternating 150 Å GaAs/150 Å $Al_{0.3}Ga_{0.7}As$ heterostructures which was grown without the use of growth interrupts.

In our second set of samples (sample type 2) grown at 600 °C, each of the superlattices was grown directly on top of a GaAs layer. There were 7 repetitions of the (4/2) structure and 11 repetitions of the (2/1) structure. These two were each grown using both 5 s and 30 s growth interrupts, the ones with shorter growth interrupts being grown first. The superlattice layers were separated from each other by one or two AlGaAs marker layers sandwiched by 200 Å thick GaAs layers. All of the superlattice and marker layers were grown on top of a region of alternating 150 Å $Al_{0.3}Ga_{0.7}As$/150 Å GaAs heterostructures where short 5 s interrupts were imposed at each interface to maintain a flat surface.

Regarding the STM images, we mention the following two points. First, the cleaved GaAs (110) surface is well known to have a simple 1×1 reconstruction with buckling of As relative to Ga atoms. Since the cleaved AlAs (110) surface should be similar, we do not expect any unusual rearrangement of the surface atoms within a superlattice region to occur upon cleavage. Hence, an STM image of a superlattice region should correspond closely to a single slice view of the bulk superlattice. Second, all images shown here are raw data without frequency filtering. With these two points in mind, we can now proceed to discuss the results.

III. RESULTS FOR (4/2) SUPERLATTICES

Shown in Fig. 1(a) is a 450 Å by 290 Å atomic-resolution filled-state STM image of the (4/2) superlattice. This superlattice was grown using 30 s of growth interrupt on top of a region of AlGaAs (sample 1). GaAs layers are clearly distinguished as the four lighter-shaded atomic rows running along the vertical direction from the two AlAs layers which appear dark due to the band gap difference of the two materials. On the left, one can see the beginning of the final 500 Å $Al_{0.3}Ga_{0.7}As$ region. Intermixing of GaAs and AlAs within a single atomic row at each superlattice interface is apparent as light and dark features alternating randomly along the vertical direction. By averaging over the vertical direction, as shown in Fig. 1(b), we can remove some of this atomic scale roughness and more easily observe general trends in the grown superlattice. Such an average is basically a simulation of the result one would obtain by using cross-sectional transmission electron microscopy (XTEM) which effectively performs a columnar average over the sample thickness. However, the signature of periodicity is clear even within a single line cut as seen in Fig. 1(c).

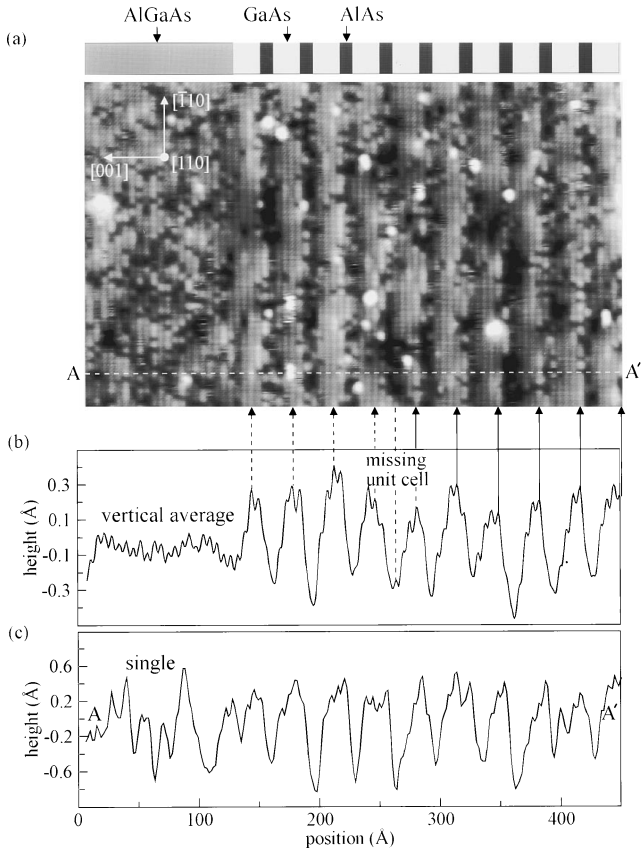

FIG. 1. (a) 450 Å×290 Å constant-current STM image of 23 Å GaAs/11 Å AlAs (4/2) superlattice of sample type 1 acquired with a sample bias of −2.25 V and a tunneling current of 0.2 nA. The total gray scale for the image is about 1.5 Å. On the left, following the last 23 Å GaAs region, is a region of $Al_{0.3}Ga_{0.7}As$. (b) Averaged line cut across the image in (a). The averaged height difference between GaAs and AlAs is typically about 0.7–0.8 Å with atomic corrugation of about 0.08 Å. Solid arrows indicate peak positions which agree with the intended device structure. Dashed arrows indicate the expected positions of peaks which appear shifted from their correct location. This shift indicates that a single unit cell has been lost during the growth near the position indicated. (c) Single line cut across the image of part (a) showing that the superlattice is well-defined at the atomic scale.

The apparent height of any particular point in the vertical average line cut is related to the ratio of the number of light features (large values) to the number of dark features (small values) along the vertical line through the image. But the

''lightness'' or ''darkness'' of the features is directly related to how the STM tip responds to a changing electronic environment. Within the superlattice section for example, the peaks within the GaAs layers show up superimposed on the ''hills'' in the line profile since the correlation of large values corresponding to GaAs builds up along the vertical direction. Averaging along the vertical direction for the AlAs layers, on the other hand, builds up the correlation of small values; they thus appear as ''valleys'' in the line profile. For the ternary AlGaAs region, one can see from the single line cut that the magnitude of the random alloy fluctuations is on the same order as the contrast across the superlattice. But since the 30% aluminum concentration is basically distributed randomly along each vertical row in the image, the average along each row comes out about the same, somewhere in between the tops of the ''hills'' and the bottoms of the ''valleys'' of the superlattice, as seen in the average line cut.

Using the average line cut, we can extract other information from the data as well. For example, for the first six periods from the right, the first GaAs layer within a single period shows up as the first small peak on the hill seen in the average line cut. The positions of these peaks are marked by the equally spaced solid arrows in the figure which point to the corresponding rows in the image. After the sixth period, we observe an effect which is very difficult to see in the image or any single line cut. While the spacing of all the arrows remains the same across the entire superlattice, the dashed arrows point to the second row within the GaAs part of each superlattice period. This indicates a shift to the right of the last four periods by one row suggesting that a row was lost somewhere between the sixth and seventh periods of the superlattice. However, it is unclear from the data whether the missing bilayers were GaAs or AlAs.

The topographic height contrast from GaAs to AlAs and back to GaAs is not steplike but rather smoothly varying. Furthermore, asymmetry in the topographic contrast at the interfaces is observed. This is not, however, the same kind of asymmetry as the roughness asymmetry between the ''normal'' and ''inverted'' interfaces described previously, for example in the case of AlGaAs/GaAs heterointerfaces.[8–11] At the interface where AlAs is grown on GaAs, the height of the individual peaks appears to drop off gradually while at the other interface they rise up quite suddenly, giving the superlattice a ''shingled'' appearance, with the shingles sloping down from right to left.

Shown in Fig. 2(a) is a zoom-in view of the (4/2) superlattice of Fig. 1. The topographic asymmetry effect is even better seen in the averaged line cut shown below in Fig. 2(b) (a slice of the image containing the two bright contamination features has been removed from the average). We label the transition which appears to be more gradual as type ''A'' and the steeper one as type ''B.'' In this case, the type A transition corresponds to the interface where AlAs is grown on GaAs while the type B transition corresponds to the interface where GaAs is grown on AlAs. The relative orientation of the cations and anions for this surface is shown in Fig. 2(c).

Next, consider the (4/2) superlattice image shown in Fig. 2(d) which was acquired using similar bias conditions as the image of Fig. 2(a) but on a different sample using a different

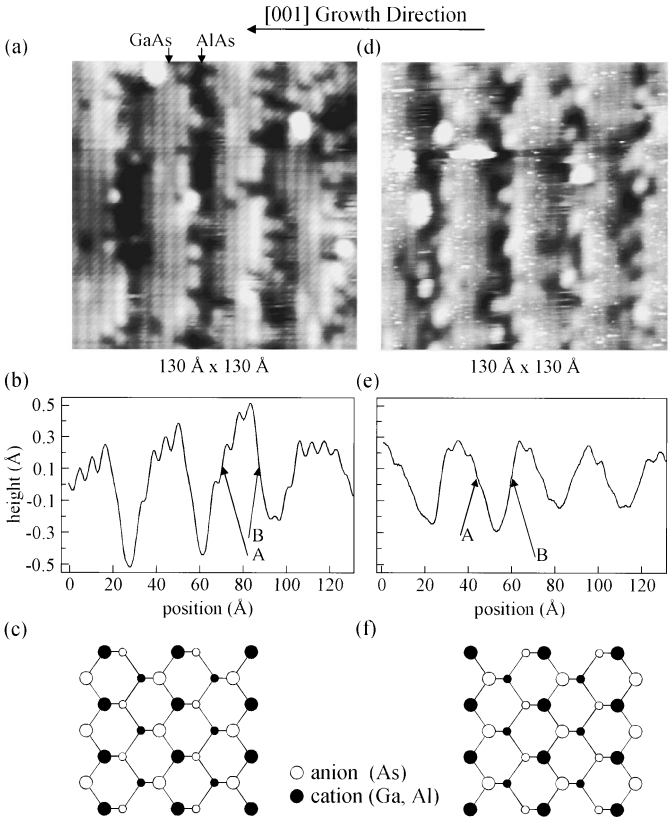

FIG. 2. (a) Small scale image of (4/2) superlattice of sample type 1. (b) Average line profile for image (a) showing ''A'' and ''B'' type transitions at the interfaces. (c) Crystal lattice orientation corresponding to image (a). (d) Image of (4/2) superlattice of sample type 2 (sample voltage -2.59 V, tunneling current 0.1 nA) with its average line cut shown in (e) and symmetry reversal indicated by the exchange of the assignment of ''A'' and ''B'' type interfaces. In (f) is shown the crystal lattice orientation corresponding to the image shown in (d).

tip. Notice that the growth direction for the samples shown in Figs. 2(a) and 2(d) is the same. But in contrast to the sample shown in Fig. 2(a), the interface where AlAs is grown on GaAs is now type B while the other interface is type A. This is seen clearly in the averaged line cut shown in Fig. 2(e). In fact, these two samples have just the opposite asymmetry. Shown in Fig. 2(f) is the relative orientation of cations and anions for the sample shown in Fig. 2(d) which is also opposite to the orientation shown in Fig. 2(c). We thus conclude that the observed asymmetry effect is primarily due to the cation-anion orientation.

We now consider an additional effect which is based on the detailed atomic bonding configurations at the interfaces. Since we are imaging the filled states of the sample surface, we are not directly probing the aluminum and gallium atoms themselves but rather the electronic effects these two atomic species have on the surface arsenic atoms. Nevertheless, Johnson *et al.*, for example, indicated that the apparent depth of an arsenic site should be dependent on its number of aluminum nearest neighbors for the filled-state image.[3] One way then to predict how much the tip should respond to the changing electronic density of states across the interface is to simply count the number of aluminum atoms bonded to surface arsenic atoms.

For a given cation-anion orientation, there are two pos-

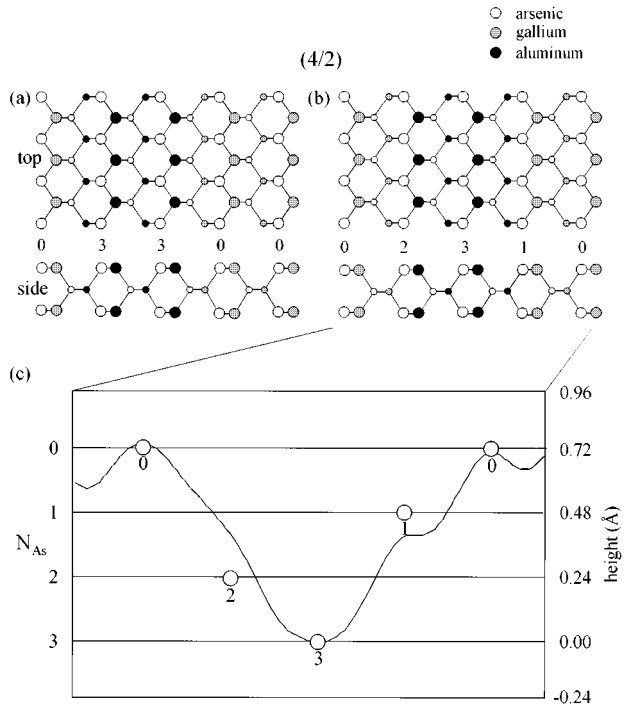

FIG. 3. Two possible surface atomic bonding models for the (4/2) superlattice are shown in (a) and (b) for a lattice orientation equivalent to (c) of Fig. 2. The average line cut across a single period of the (4/2) superlattice of Fig. 2(a) is plotted in (c), which correlates remarkably well with the number of aluminum atoms bonded to surface arsenic atoms, N_{As}, for the asymmetric bonding model.

sible atomic models for a *perfect* (4/2) superlattice, as shown in Figs. 3(a) and 3(b). In these two models, arsenic atoms are represented as open circles, gallium atoms as shaded circles, and aluminum atoms as solid circles. Each period of the (4/2) superlattice contains 4 bilayers of aluminum. The first model, shown in Fig. 3(a), has the first (in order of growth direction) of the four aluminum bilayers intersecting the (110) surface along a surface zig-zag chain. Once the positioning of this bilayer is assigned, there are no other arbitrary choices to be made regarding the model. In the second model, shown in Fig. 3(b), the first of the four aluminum bilayers intersects the surface along a second-layer-down zig-zag chain, and the rest of the model is then completely determined. For the other anion-cation orientation, we obtain equivalent but mirrored lattice models. Furthermore, it is important to realize that the difference between the two models is only a single (110) plane of atoms. Cleaving a crystal produces two fresh cleavage faces. If one face is of the type shown in Fig. 3(a), then the other *must* be of the type shown in Fig. 3(b).

We can now count the number of aluminum atoms bonded to surface arsenic atoms. In the case of the model shown in Fig. 3(a), we obtain the very symmetric-looking sequence {...0000330000330000...}, which does not seem to explain the asymmetric-appearing profiles in the data. On the other hand, the model shown in Fig. 3(b) gives us the asymmetric-looking sequence {...000231000231000...}, which seems to agree with the appearance of the data at least in a qualitative way. If we now simply take this result at face value and plot these numbers as a function of position across the interface together with an actual line profile for the (4/2) superlattice, we obtain a reasonably good agreement as seen in part (c) of Fig. 3. Despite the success of this comparison, this is not yet a complete picture since, as suggested above, there is no reason why we should not observe the more symmetric superlattice. After all, every cleave produces both kinds of surfaces.

As mentioned previously, the (4/2) superlattice shown in Figs. 1 and 2(a) was grown using a 30 s growth interrupt on top of an AlGaAs layer. The (4/2) superlattice grown on top of AlGaAs using only 5 s of growth interrupt was not distinguishable from a ternary AlGaAs region. The (4/2) superlattice shown in Fig. 2(d), on the other hand, was grown using only a 5 s growth interrupt. Although the image quality is not excellent due to the STM tip condition, the periodicity appears to be just as good as that seen in Fig. 2(a) for the 30 s growth interrupt. The key difference is that this superlattice was grown on top of a layer of GaAs. It seems, therefore, that the material on which these short period superlattices are grown plays an important role in the interface formation. In this case, the result implies that GaAs is a superior substrate material compared with AlGaAs.

IV. RESULTS FOR (2/1) SUPERLATTICES

The atomic resolution image for the 5 s (2/1) superlattice grown on top of a layer of GaAs is diplayed in Fig. 4(a). The device structure is indicated at the top where each dark rectangle represents one unit cell of AlAs. While the image looks faintly periodic, the periodicity does not show very clearly for a single line cut as shown in Fig. 4(c). However, averaging along the vertical direction can be used to boost up the coherence, resulting in the nicely periodic profile shown in Fig. 4(b). While there does appear to be a shift to the right for several of the peaks, similar to what was seen in the (4/2) superlattice shown in Fig. 1, most of the peaks line up perfectly with their expected positions. Here is a case in point where a signal averaging technique (such as XTEM) can reveal a very beautiful, periodic looking superlattice while locally it is really not so good due to fluctuations at the atomic scale.

On the other hand, the vertical average profile reveals that the (2/1) superlattice also exhibits topographic asymmetry as was seen in the case of the (4/2) superlattice. A similar counting analysis can be applied to try to understand the origin of this observed asymmetry. This has been done, and the results are shown in Fig. 5. Figure 5(a) is the more asymmetric of the two possible atomic models and shows 2 bilayers of aluminum atoms sandwiched in between bilayers of gallium atoms. Counting the number of aluminum atoms bonded to surface arsenic atoms, we obtain the asymmetrical sequence {...0210210...} as opposed to {...00300300...} which would be obtained if the other model was used. This has been plotted together with the averaged line cut data for a single period of the (2/1) superlattice in (b). Similar to the case of the (4/2), the agreement between this simple-minded counting and the actual data is quite good.

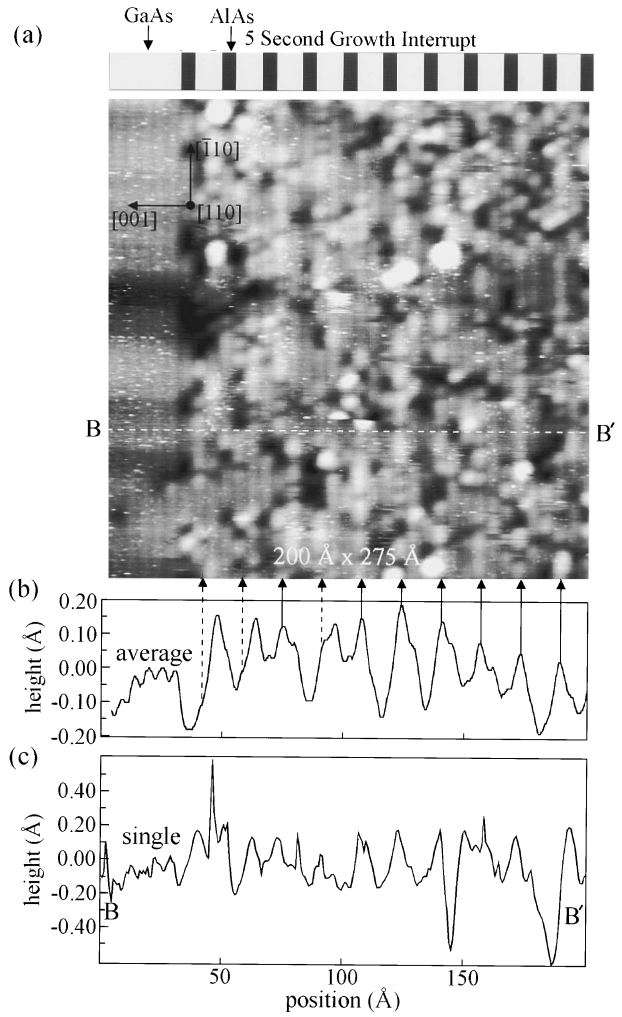

FIG. 4. (a) 200 Å×200 Å STM image of the (2/1) superlattice of sample type 2 acquired with a sample bias of −2.59 V and a tunneling current of 0.1 nA. In the device structure indicated, each dark rectangle represents a single unit cell of AlAs. The superlattice periodicity can be seen faintly in the image where about every third row appears slightly brighter despite many fluctuations. (b) Vertical averaging boosts up the coherence resulting in peaks, most of which line up perfectly with their expected positions according to the intended device structure. In addition, several of the peaks indicated with dashed arrows appear to be shifted to the right by one unit cell from their expected positions. (c) A single line cut showing that the superlattice is not well-defined at the atomic scale.

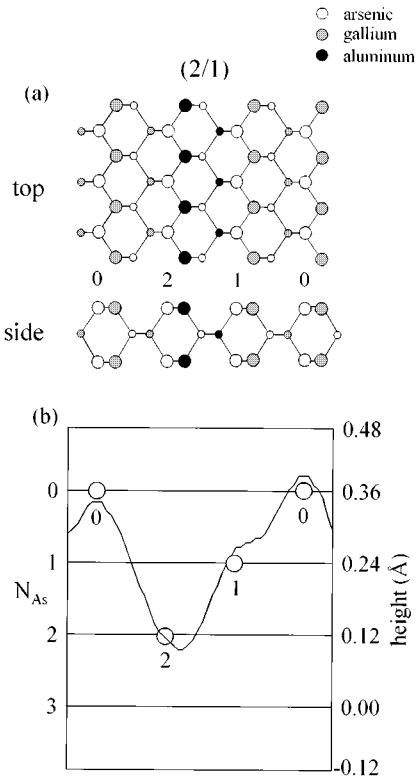

FIG. 5. Asymmetric surface atomic bonding model for the (2/1) superlattice is shown in (a). The number of aluminum atoms bonded to surface arsenic atoms, N_{As}, is plotted together with the averaged line cut data for a single period of the (2/1) superlattice in (b).

V. CONCLUSION

We have used the method of cross-sectional STM to investigate the influence of key growth parameters on the resulting interfacial quality of AlAs/GaAs short period superlattices. We find that there are two essential conclusions. The first is that when growing superlattices on top of AlGaAs, periodicity shorter that 4 unit cells of GaAs and 2 unit cells of AlAs and growth interrupts shorter that 30 s makes the superlattice difficult if not impossible to observe at the atomic scale. Second, when the same superlattices are grown on top of GaAs using as little as 5 s of growth interrupt, they can be resolved very nicely, indicating that the growth parameters are sufficient for the formation of abrupt interfaces for this substrate material. We conclude that the material on which the superlattices are grown is very important. In particular, GaAs as a substrate material seems to provide a smoother starting surface compared with AlGaAs. In addition, we have found that the superlattices seem to have a characteristic line profile which depends on the relative orientation of the cations and anions. We have also discussed some simple models of short period superlattices and from these models made some comparisons with our experimental STM results.

Finally, it is interesting that we have not yet observed the more symmetrical structure in our data. Understandably, the first sample set (superlattices grown on AlGaAs) was studied many times in the attempt to observe the ultrashort (2/1) superlattice, always without success. However, after obtaining the new sample set (superlattices grown on GaAs), the first data run already revealed the (2/1) superlattice grown with only 5 s of growth interrupt. While further experiment may be able to achieve slightly better image quality, it will not change the primary conclusions of this work but might be able to verify the observation of the symmetric structure, as discussed.

ACKNOWLEDGMENTS

This work was partly supported by the National Science Foundation (Grant No. DMR-94-02938), a Texas Instruments University Research Grant, the Trull Centennial Professorship in Physics Fellowship No. 1, the Texas Advanced Research Program, the Joint Services Electronics Program

(Contract No. AFOSR F49620-92-C-0027), and the Science and Technology Center Program of the National Science Foundation (Grant No. CHE8920120).

[1]E. E. Mendez and G. Bastard, Phys. Today **46** (6), 34 (1993).
[2]L. L. Chang and L. Esaki, Phys. Today **45** (10), 36 (1992).
[3]O. Albrektsen, D. J. Arent, H. P. Meier, and H. W. M. Salemink, Appl. Phys. Lett. **57,** 31 (1990).
[4]M. B. Johnson, U. Maier, H.-P. Meier, and H. W. M. Salemink, Appl. Phys. Lett. **63**, 1273 (1993).
[5]H. W. M. Salemink and O. Albrektsen, Phys. Rev. B **47**, 16044 (1993).
[6]H. W. M. Salemink, O. Albrektsen, and P. Koenraad, Phys. Rev. B **45**, 6946 (1992).
[7]R. M. Feenstra, Phys. Rev. B **50**, 4561 (1994).
[8]A. R. Smith, S. Gwo, K. Sadra, Y. C. Shih, B. G. Streetman, and C. K. Shih, J. Vac. Sci. Technol. B **12**, 2610 (1994).
[9]S. Gwo, K.-J. Chao, C. K. Shih, K. Sadra, and B. G. Streetman, Phys. Rev. Lett. **71**, 1883 (1993).
[10]S. Gwo, K.-J. Chao, A. R. Smith, C. K. Shih, K. Sadra, and B. G. Streetman, J. Vac. Sci. Technol. B **11**, 1509 (1993).
[11]R. M. Feenstra, D. A. Collins, D. Z.-Y Ting, M. W. Wang, and T. C. McGill, Phys. Rev. Lett. **72**, 2749 (1994).
[12]A. Y. Lew, E. T. Yu, D. H. Chow, and R. H. Miles, Appl. Phys. Lett. **65**, 201 (1994).
[13]A. R. Smith, K. J. Chao, C. K. Shih, Y. C. Shih, and B. G. Streetman, Appl. Phys. Lett. **66**, 478 (1995).